ELSEVIER

Inorganica Chimica Acta 223 (1994) 43–53

Inorganica Chimica Acta

Synthesis, structure and stability of complexes of lanthanide nitrates with $[(MeO)_2P(O)]_2C(OH)Ph$ and the isomeric $(MeO)_2P(O)OCHPhP(O)(OMe)_2$

Andrew W.G. Platt[a,*], David Simpson[a], John Fawcett[b], David R. Russell[b]

[a]*Chemistry Division, Staffordshire University, College Road, Stoke-on-Trent ST4 2DE, UK*

[b]*Department of Chemistry, The University, Leicester LE1 7RH, UK*

Received by Editor 27 January 1994; received by Publisher 6 April 1994

Abstract

The syntheses of compounds $Ln(NO_3)_3L_2$ (**A1–A12**) and $Ln(NO_3)_3L'_2$ (**B1–B12**), where $L=[(MeO)_2P(O)]_2C(OH)Ph$ and $L'=(MeO)_2P(O)OCHPhP(O)(OMe)_2$ and Ln = La–Lu except Pm, Tb and Tm, are described. For the heavier lanthanides isomerisation of **A** to **B** occurs readily in solution. All compounds are prone to loss of methyl nitrate above ambient temperature, the propensity for this reaction increasing with the atomic weight of the metal. Study by IR and NMR spectroscopies indicate that both the series **A** and **B** show slight differences in structure between the heavier and lighter lanthanides and that these differences are probably due to changes in the coordination of the nitrate ligands. The X-ray structures of two isomeric praseodymium complexes **A3** ($R'=0.0690$ for 5326 diffractometer observed reflections) and **B3** ($R'=0.0393$ for 4427 diffractometer observed reflections) show that in both cases the metals are ten-coordinated. The hydrogen atoms of the OH group in **A3** were not located but appear to be hydrogen bonded to two of the nitrate groups. One of the ligands in **A3** is distorted towards the structure of the isomer. The isomerisations of complexes **A** to **B** are discussed in terms of the electrostatic interactions between the phosphorus atoms and the metal centre.

Keywords: Crystal structures; Lanthanide complexes; Bidentate ligand complexes; Phosphoryl complexes

1. Introduction

Whilst the coordination chemistry of phosphoryl compounds with lanthanide metals has been thoroughly studied [1] complexes of bidentate analogues are less well represented.

Complexes of lanthanide nitrates with $[(R_2P(O)]_2CH_2$ [2,3] and $[(Me_2N)_2P(O)]_2NMe$ [4,5] have been characterised, whilst others are presumably involved in solvent extraction using $[(RO)_2P(O)]_2CH_2$ in nitrate media [6].

The recent fortuitous synthesis, albeit in low yield, of complexes **A1** and **A2** by the reaction of $(MeO)_2P(O)C(O)Ph$ with lanthanum and cerium nitrates in methanol [7] prompted us to study the direct reactions of the ligand **L** and its isomer **L′** with lanthanide nitrates.

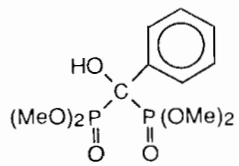

L

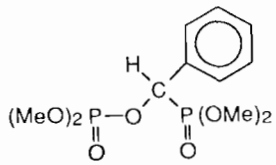

L′

2. Results and discussion

2.1. Preparation of the complexes

The direct reaction of L with lanthanum nitrate in methanol gave only a modest improvement in the yield

*Corresponding author.

SSDI 0020-1693(94)03988-Z

from 20 to 35% and although the praseodymium complex could be obtained in lower yield (~10%) the complexes of the heavier lanthanides could not be crystallised from methanol. Of the common organic solvents, acetonitrile was found to be the best for the synthesis of complexes **A**. The characterisation data are given in Table 1. Reaction of a slurry of L with solutions of the lighter lanthanide (La–Eu) nitrates gave clear solutions from which the products crystallised spontaneously in 80–60% yield. For gadolinium and subsequent metals the product was more soluble and the crude product was isolated by evaporation of the solvent under reduced pressure followed by precipitation with diethyl ether from chloroform solution. The yields using this procedure were generally lower, at about 50% for Gd and Dy, with the title compounds not being obtained for the heavier metals as discussed below.

The difficulties encountered with the heavier lanthanides are thought to be due to the increased solubility and the tendency of the complexes to undergo isomerisation. In all preparations it was found that isomerisation of L to L′ occurred as a side reaction and that the rate of this reaction increased as the lanthanide series was traversed. The base catalysed isomerisation of L to L′ is known to be rapid [8], but hydroxybisphosphonates are stable to acids, the free phosphonic acid being obtainable by reflux with concentrated HCl [9]. This isomerisation is discussed in terms of the structures below. Complexes of L with ytterbium and lutetium nitrates could not be obtained. 2:1 mixtures of L with ytterbium and lutetium nitrates examined by ^{31}P NMR spectroscopy showed that initial complex formation was followed by rapid isomerisation, indicated by the observation of two doublets for L′, this process being complete within 45 min. The process is slower for the lighter metals, isomerisation of $Eu(NO_3)_3L_2$ to $Eu(NO_3)_3L'_2$ being complete within one week in acetonitrile solution.

The complexes **B** are all more soluble than the isomeric **A** series and were isolated by precipitation from acetonitrile with diethyl ether for the early lanthanides or by evaporation of the acetonitrile followed by recrystallisation from chloroform/diethyl ether for the heavier metals. Characterisation data are given in Table 2.

For both series of complexes it was found that satisfactory elemental analyses corresponding to $Ln(NO_3)_3L_2$ could not be obtained for holmium and subsequent elements. Attempts to prepare analytically pure samples of these 2:1 complexes by slow diffusion of diethyl ether into chloroform solutions of the crude complexes gave solids with an apparent 1:1 ligand to metal ratio. Although elemental analyses are not entirely satisfactory (see Experimental) it seems that binuclear, or more complex species, are formed with a composition approximating to $Ln_2(OH)_2(NO_3)_4L_2$ or $Ln_2O(NO_3)_4L_2$. The hydroxo and oxo bridges are presumably derived from moisture in the solvent. Optimisation of the conditions for formation of these complexes requires further work and is still under investigation.

Evidence that holmium and erbium do form genuine 2:1 complexes can be seen from the general similarity

Table 1
Characterisation data for complexes **A**

Complex	Ln	Analysis: found(calc.) (%)			$\delta\,^{31}P$ (CH_3CN)	$\Delta\nu_{1/2}$[a]
		C	H	N		
A1	La	[b]			18.4	< 10
A2	Ce	[b]			30.0	40
A3	Pr	26.63(27.09)	3.69(3.72)	3.98(4.31)	45.6	90
A4	Nd	27.24(27.00)	3.92(3.71)	3.63(4.29)	55.8	50
A5	Sm	27.16(26.82)	3.75(3.68)	4.00(4.26)	16.3	40
A6	Eu				−50.6	80
A7	Gd				not observed	
A8	Dy	27.05(26.50)	3.65(3.64)	3.84(4.20)	−107	600
A9	Ho	[c]			−71	460
A10	Er	[c]			−65	890
A11	Yb	[d]			−3.8	150
A12	Lu	[d]			16.0	< 10

IR data (KCl or KBr discs). All isolated complexes show strong bands characteristic of bidentate nitrate groups between 1500–1475 and 1320–1290 cm^{-1}; both these bands were observed to have a doublet structure. The absorbance due to the P=O group was between 1220 and 1205 cm^{-1} compared with 1265 and 1220 cm^{-1} for the free ligand.

[a]Linewidth at half height (Hz).

[b]Samples had identical IR and NMR spectra with those prepared using methanol as solvent for which satisfactory analyses have already been obtained (see Ref. [7]).

[c]Analytically pure samples could not be obtained, see Sections 2 and 3.

[d]Observed in solution only.

Table 2
Characterisation data for complexes **B**

Complex	Ln	Analysis: found(calc.) (%)			^{31}P data ($CDCl_3$) $(MeO)_2P_A(O)OCH(Ph)P_B(O)(OMe)_2$			
		C	H	N	δ_A	$\Delta\nu_{1/2}$[a]	δ_B	$\Delta\nu_{1/2}$
B1	La	27.43(27.15)	3.75(3.73)	4.00(4.32)	0.4	<10	18.4	<10[b]
B2	Ce	26.93(27.11)	3.62(3.72)	3.74(4.31)	22.4	30	41.1	30
B3	Pr	26.97(27.09)	3.93(3.72)	4.00(4.31)	48.2	50	64.4	50
B4	Nd	26.43(27.00)	3.85(3.71)	4.10(4.29)	70.2	30	82.4	30
B5	Sm	25.87(26.82)	3.69(3.68)	3.72(4.26)	−2.5	<10	16.5	<10[c]
B6	Eu	26.71(26.79)	3.76(3.68)	4.10(4.26)	−85	300	−51	250
B7	Gd	26.83(26.64)	3.74(3.66)	4.05(4.23)	not observed			
B8	Dy	25.98(26.50)	3.65(3.64)	3.75(4.21)	−238	1500	−118	1400
B9	Ho		[d]		−173	920	−90	660
B10	Er		[d]		−165	660	−119	310
B11	Yb		[d]		−33.9	150	−16.9	110
B12	Lu		[e]		1.0	<10	17.1	<10[f]

IR data (KCl or KBr discs). Complexes **B1–B7** showed two characteristic strong bands due to coordinated nitrate between 1490–1450 and 1320–1300 cm^{-1}, both of these bands have a doublet structure. In complex **B8** the doublet separation for the 1320–1300 cm^{-1} band is smaller, whilst in **B9–B11** this band appeared as a singlet. All complexes gave a strong absorbance due to the P=O groups between 1245 and 1250 cm^{-1} compared with 1275 cm^{-1} for the free ligand.

[a]Linewidth at half height (Hz).

[b]^3J(PP) 27 Hz.

[c]^3J(PP) 30 Hz.

[d]Analytically pure samples could not be obtained (see Sections 2 and 3).

[e]Observed in solution.

[f]^3J(PP) 29 Hz.

of the IR spectra of the crude complexes with those of their lighter congeners, and in particular, the absence of the two P=O absorptions associated with the free ligand indicates that the crude products are not simply mixtures of 1:1 complexes and excess L.

2.2. Structures

The structures of the praseodymium complexes **A3** and **B3** are shown in Figs. 1 and 2, respectively. Selected bond lengths and angles are given in Tables 3–6 and the atomic coordinates in Tables 7 and 8. The structures show that in both cases the praseodymium is ten-coordinate with all ligands chelating through two oxygen atoms. The overall geometry of **A3** is very similar to the related $La(NO_3)_3(NIPA)_2$ (NIPA = $[(Me_2N)_2P(O)]_2$-NMe) [5].

The ranges of Pr–O (nitrate) distances, 2.531–2.659 Å in **A3** and 2.568–2.658 Å in **B3**, compare well with the interatomic distances observed for other simple ten-coordinate praseodymium nitrate complexes, such as $Pr(NO_3)_3(dmso)_4$ (2.605–2.756 Å) [10], the $Pr(NO_3)_3(OH_2)_4$ unit in $Pr(NO_3)_3(OH_2)_4 \cdot (bipy)_2 \cdot H_2O$ (2.52–2.75 Å) [11] and a praseodymium nitrate complex of an aza crown ether (2.608–2.678 Å) [12]. The N–O(Pr) distances lie well within the observed range for the above examples, but the terminal N–O bond lengths at 1.216–1.177 Å in **A3**, seem to be shorter, the typical distances in the examples cited above being around 1.24 Å.

Although the hydrogen atoms of the OH groups of **A3** were not detected there is evidence that they are involved in intramolecular hydrogen bonding to the nitrate groups. Atom O(2) seems to be hydrogen bonded to O(9A) whilst O(2A) is H bonded to O(8A). The OH group in the free ligand is hydrogen bonded to one of the phosphoryl groups. The O···O distance between the two hydrogen-bonded oxygen atoms is 2.735 Å [13] compared with 2.715 Å for O(8A)···O(2A) and 2.721 Å for O(2)···O(9B) in **A3**. The hydrogen bonding causes the nitrate ligands to bond asymmetrically to the metal. Thus the Pr–O(nitrate) distances for the oxygens involved in hydrogen bonding (Pr–O(8A) and Pr–O(9B)) are significantly longer than the other Pr–O(nitrate) distances (Pr–O(9) and Pr–O(8B)) whilst for nitrate C, which is not involved in hydrogen bonding, the Pr–O distances are not significantly different from each other.

No hydrogen bonding is possible in **B3** and the nitrate ligands show less distortion. The ranges of Pr–O(nitrate), N–O(Pr) and N–O(terminal) are all much narrower than in **A3**, in particular the N–O(Pr) lengths only vary by 1.4% around the mean compared with 5% in **A3**.

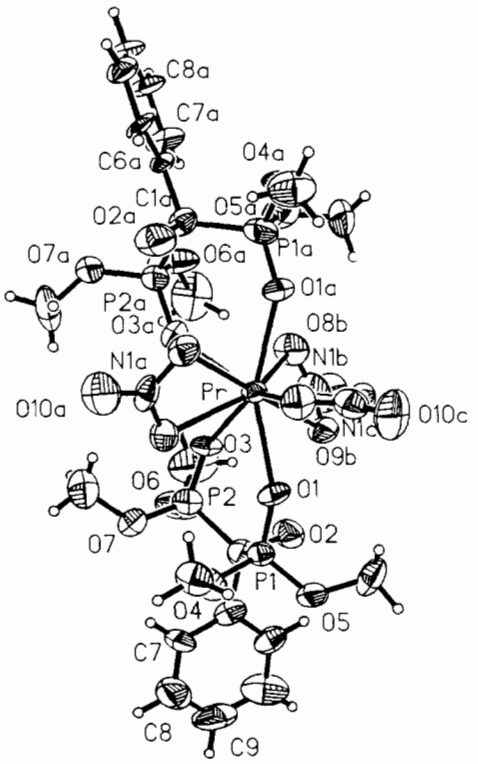

Fig. 1. Structure of complex **A3** (hydrogen atom labels omitted for clarity).

Table 3
Bond lengths (Å) in complex **A3**

Pr–O(1)	2.434(9)	Pr–O(3)	2.498(9)
Pr–O(1A)	2.475(9)	Pr–O(3A)	2.487(8)
Pr–O(8A)	2.630(14)	Pr–O(9A)	2.531(12)
Pr–O(8B)	2.565(13)	Pr–O(9B)	2.659(14)
Pr–N(1C)	3.006(14)	Pr–O(8C)	2.558(10)
Pr–O(9C)	2.582(10)	P(1)–O(1)	1.476(10)
P(1)–O(4)	1.538(11)	P(1)–O(5)	1.538(11)
P(1)–C(1)	1.860(16)	P(2)–O(3)	1.480(9)
P(2)–O(6)	1.536(15)	P(2)–O(7)	1.544(15)
P(2)–C(1)	1.811(14)	O(2)–C(1)	1.404(19)
O(4)–C(2)	1.422(23)	O(5)–C(3)	1.445(21)
O(6)–C(4)	1.444(25)	O(7)–C(5)	1.411(27)
C(1)–C(6)	1.551(21)	C(6)–C(7)	1.375(21)
C(6)–C(11)	1.403(30)	C(7)–C(8)	1.378(29)
C(8)–C(9)	1.340(41)	C(9)–C(10)	1.424(33)
C(10)–C(11)	1.318(29)	P(1A)–O(1A)	1.469(10)
P(1A)–O(4A)	1.592(14)	P(1A)–O(5A)	1.540(12)
P(1A)–C(1A)	1.832(15)	P(2A)–O(3A)	1.482(9)
P(2A)–O(6A)	1.536(15)	P(2A)–O(7A)	1.538(13)
P(2A)–C(1A)	1.861(15)	O(2A)–C(1A)	1.470(20)
O(4A)–C(2A)	1.413(25)	O(5A)–C(3A)	1.502(25)
O(6A)–C(4A)	1.388(30)	O(7A)–C(5A)	1.483(24)
C(1A)–C(6A)	1.500(20)	C(6A)–C(7A)	1.409(22)
C(6A)–C(11A)	1.403(28)	C(7A)–C(8A)	1.369(25)
C(8A)–C(9A)	1.337(34)	C(9A)–C(10A)	1.412(23)
C(10A)–C(11A)	1.356(22)	N(1A)–O(8A)	1.274(15)
N(1A)–O(9A)	1.277(26)	N(1A)–O(10A)	1.177(24)
N(1B)–O(8B)	1.262(31)	N(1B)–O(9B)	1.271(17)
N(1B)–O(10B)	1.182(28)	N(1C)–O(8C)	1.229(19)
N(1C)–O(9C)	1.292(21)	N(1C)–O(10C)	1.216(18)

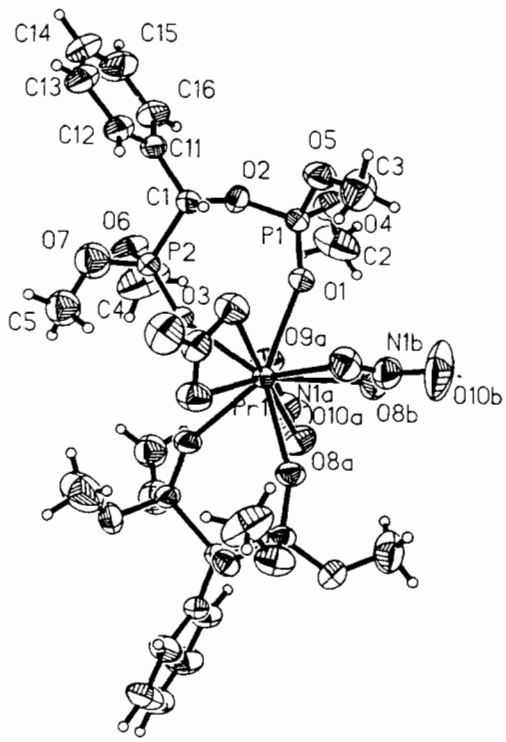

Fig. 2. Structure of complex **B3** (hydrogen atom labels omitted for clarity). The molecule has crystallographic two-fold symmetry.

It is interesting to compare the structure of coordinated L with that of the free ligand [13]. The formation of the chelate ring disrupts the hydrogen bonding in the ligand and also brings the two phosphorus atoms into closer proximity. Thus on coordination the P···P distance decreases from 3.055 Å in L to 3.016 and 3.033 Å. These are similar to the P···P distance of 3.019 Å in $La(NO_3)_3(NIPA)_2$ [5]. In the coordinated ligand where the P···P distance is the largest the structure appears to be distorted towards that of the isomeric L′. Thus the distorted ligand has a relatively long C(1A)–O(2A) bond at 1.470 Å compared with 1.404 Å for C1–O1 in the coordinated 'undistorted' phosphonate and 1.426 Å in the free ligand. This lengthening of the C–O bond is associated with a narrowing of the O(2A)–C(1A)–P(2A) angle, which at 99.9° is 4° less than the average of the other O–C–P angles, and a slightly shorter non-bonded distance between the hydroxyl oxygen O(2A) and P(2A) of the phosphoryl group (2.561 Å as opposed to 2.609 Å for O(2A)–P(1A) in the same ligand). These distortions, when taken to their full extent would lead to the production of the isomeric L′. This process is probably driven by the increased electrostatic repulsion between the two positive phosphorus centres, the production of the isomer allowing a greater P···P separation. The P···P distance increases from an average of 3.025 Å

Table 4
Selected bond angles (°) for complex **A3**

O(1)–Pr–O(3)	72.1(3)	O(1)–Pr–O(1A)	148.9(3)
O(3)–Pr–O(1A)	137.3(3)	O(1)–Pr–O(3A)	136.7(3)
O(3)–Pr–O(3A)	70.6(3)	O(1A)–Pr–O(3A)	73.6(3)
O(1)–Pr–O(8A)	110.2(3)	O(3)–Pr–O(8A)	115.7(3)
O(1A)–Pr–O(8A)	70.1(3)	O(3A)–Pr–O(8A)	68.7(3)
O(1)–Pr–O(9A)	72.6(4)	O(3)–Pr–O(9A)	75.5(4)
O(1A)–Pr–O(9A)	118.4(4)	O(3A)–Pr–O(9A)	77.5(3)
O(8A)–Pr–O(9A)	48.8(4)	O(1)–Pr–O(8B)	117.4(5)
O(3)–Pr–O(8B)	76.8(4)	O(1A)–Pr–O(8B)	71.6(4)
O(3A)–Pr–O(8B)	73.9(4)	O(8A)–Pr–O(8B)	132.2(4)
O(9A)–Pr–O(8B)	145.3(4)	O(1)–Pr–O(9B)	69.8(3)
O(3)–Pr–O(9B)	66.5(3)	O(1A)–Pr–O(9B)	108.6(3)
O(3A)–Pr–O(9B)	112.9(3)	O(8A)–Pr–O(9B)	177.7(3)
O(9A)–Pr–O(9B)	132.8(4)	O(8B)–Pr–O(9B)	48.0(4)
O(1)–Pr–N(1C)	71.0(3)	O(3)–Pr–N(1C)	141.3(3)
O(1A)–Pr–N(1C)	78.0(3)	O(3A)–Pr–N(1C)	147.9(4)
O(8A)–Pr–N(1C)	87.9(4)	O(9A)–Pr–N(1C)	103.9(4)
O(8B)–Pr–N(1C)	110.8(4)	O(9B)–Pr–N(1C)	90.0(4)
O(1)–Pr–O(8C)	72.8(3)	O(3)–Pr–O(8C)	142.6(3)
O(1A)–Pr–O(8C)	79.8(3)	O(3A)–Pr–O(8C)	132.9(4)
O(8A)–Pr–O(8C)	65.9(3)	O(9A)–Pr–O(8C)	82.1(3)
O(8B)–Pr–O(8C)	132.2(3)	O(9B)–Pr–O(8C)	112.1(4)
N(1C)–Pr–O(8C)	23.8(4)	O(1)–Pr–O(9C)	73.5(3)
O(3)–Pr–O(9C)	129.0(4)	O(1A)–Pr–O(9C)	77.5(3)
O(3A)–Pr–O(9C)	149.2(3)	O(8A)–Pr–O(9C)	111.0(4)
O(9A)–Pr–O(9C)	126.8(4)	O(8B)–Pr–O(9C)	87.1(4)
O(9B)–Pr–O(9C)	66.8(4)	N(1C)–Pr–O(9C)	25.3(4)
O(8C)–Pr–O(9C)	49.1(4)	O(1)–P(1)–C(1)	109.8(6)
Pr–O(1)–P(1)	147.6(5)	Pr–O(3)–P(2)	143.1(5)
P(1)–C(1)–O(2)	104.2(8)	P(1)–C(1)–P(2)	110.5(9)
P(2)–C(1)–O(2)	105.5(9)	Pr–O(1A)–P(1A)	141.7(5)
Pr–O(3A)–P(2A)	145.9(5)	P(1A)–C(1A)–P(2A)	110.4(9)
P(1A)–C(1A)–O(2A)	103.8(9)	P(2A)–C(1A)–O(2A)	99.9(8)
Pr–O(8A)–N(1A)	96.3(11)	Pr–O(9A)–N(1A)	101.0(8)
Pr–O(9B)–N(1B)	95.0(13)	Pr–O(8B)–N(1B)	99.9(9)
Pr–N(1C)–O(9C)	58.7(7)	Pr–N(1C)–O(8C)	57.2(7)
Pr–N(1C)–O(10C)	174.4(11)	Pr–O(8C)–N(1C)	99.0(10)
Pr–O(9C)–N(1C)	96.0(9)		

in **A3** to 3.642 Å in the isomeric **B3**. Indeed on isomerisation not only does the P···P distance increase but the P···Pr distances also increase from an average of 3.775 Å in **A3** to 3.830 Å in **B3**, further reducing the electrostatic repulsions between positive centres. The fact that the heavier lanthanide ions promote isomerisation more readily is consistent with this view as chelation with smaller metals would bring the phosphoryl groups closer to each other and to the metal thus increasing the electrostatic repulsions. In addition the higher charge density on the smaller lanthanide ions might be expected to increase the positive charge on the phosphorus atom and hence promote the formation of the phosphate P–O bond. A combination of these factors probably accounts for the fact that $Yb(NO_3)_3L_2$ and $Lu(NO_3)_2L_2$ cannot be isolated, and the difficulties in obtaining pure samples of the holmium and erbium complexes.

2.3. Thermal stability

All the isolable complexes are stable as solids at room temperature. Complexes in series **A** show no tendency to isomerise in the solid state, although isomerisation does occur in solution. For example, samples stored at room temperature for up to 6 months show no sign of contamination with **B** when their solutions are examined by ^{31}P NMR.

Considerable differences in thermal stability are observed at above ambient temperatures. Thus whilst all complexes decompose violently on melting between 130 and 140 °C with evolution of gas, at 120 °C decomposition occurs gradually with apparent loss of nitrate for both **A** and **B** and with additional isomerisation of **L** to **L'** for series **A**. The loss of nitrate is evident from the absence of characteristic absorbances due to coordinated or ionic nitrate in the IR spectra, and the failure to detect nitrogen in microanalysis of the products. The

Table 5
Bond lengths (Å) in complex **B3**

Pr(1)–O(1)	2.459(2)	Pr(1)–O(3)	2.460(2)
Pr(1)–O(8A)	2.658(5)	Pr(1)–O(9A)	2.568(4)
Pr(1)–N(1B)	2.989(5)	Pr(1)–O(8B)	2.581(4)
Pr(1)–O(1A)	2.459(2)	Pr(1)–O(3A)	2.460(2)
Pr(1)–O(8AA)	2.658(5)	Pr(1)–O(9AA)	2.568(4)
Pr(1)–O(8BA)	2.581(4)	P(1)–O(1)	1.460(2)
P(1)–O(2)	1.566(3)	P(1)–O(4)	1.533(4)
P(1)–O(5)	1.557(4)	P(2)–O(3)	1.467(2)
P(2)–C(1)	1.815(3)	P(2)–O(6)	1.553(4)
P(2)–O(7)	1.543(5)	O(2)–C(1)	1.463(6)
C(1)–C(11)	1.498(5)	O(4)–C(2)	1.404(10)
O(5)–C(3)	1.425(7)	O(6)–C(4)	1.396(11)
O(7)–C(5)	1.429(6)	C(11)–C(12)	1.398(8)
C(11)–C(16)	1.379(6)	C(12)–C(13)	1.396(6)
C(13)–C(14)	1.366(8)	C(14)–C(15)	1.368(11)
C(15)–C(16)	1.387(7)	N(1A)–O(8A)	1.245(5)
N(1A)–O(9A)	1.263(5)	N(1A)–O(10A)	1.220(8)
N(1B)–O(8B)	1.252(5)	N(1B)–O(10B)	1.215(8)
N(1B)–O(8BA)	1.252(5)		

gaseous products from the decomposition of **A1** and **B3** were found to be identical by IR spectroscopy. The spectra do not correspond to any simple nitrogen oxide [14] but are identical with the literature spectra reported for methyl nitrate [15] with intense bands at 1680, 1660, 1280, 1015 and 855 cm^{-1}. Elemental analysis of the residual solid gives the expected composition for loss of $3MeNO_3$. *Anal.* Found: C, 30.44; H, 3.67. Calc. for $La(NO_3)_3L_2 - 3CH_3NO_3$: C, 30.74; H, 3.67%.

The solid residues dissolve slowly in water and ^{31}P NMR spectra indicate the presence of mixed phosphate–phosphonate species in at least three distinct environments with signals at δ 27.2, 0.5 ^3J(PP) 35 Hz; δ 13.4, 2.1 ^3J(PP) 32 Hz and δ 15.4, 1.0 ^3J(PP) 20 Hz. We tentatively assign these to ionic species such as

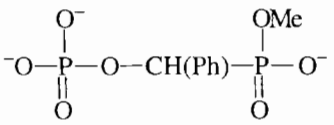

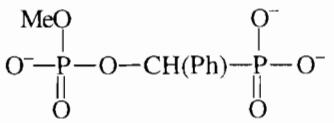

Table 6
Selected bond angles (°) for complex **B3**

O(1)–Pr(1)–O(3)	74.0(1)	O(1)–Pr(1)–O(8A)	108.8(1)
O(3)–Pr(1)–O(8A)	113.4(1)	O(1)–Pr(1)–O(9A)	74.1(1)
O(1)–Pr(1)–O(9A)	72.3(1)	O(8A)–Pr(1)–O(9A)	48.3(1)
O(3)–Pr(1)–N(1B)	71.1(1)	O(3)–Pr(1)–N(1B)	143.4(1)
O(8A)–Pr(1)–N(1B)	88.3(1)	O(9A)–Pr(1)–N(1B)	107.7(1)
O(1)–Pr(1)–O(8B)	71.5(1)	O(3)–Pr(1)–O(8B)	142.6(1)
O(8A)–Pr(1)–O(8B)	65.9(1)	O(9A)–Pr(1)–O(8B)	84.6(1)
N(1B)–Pr(1)–O(8B)	24.6(1)	O(1)–Pr(1)–O(1A)	142.2(1)
O(3)–Pr(1)–O(1A)	142.7(1)	O(8A)–Pr(1)–O(1A)	70.0(1)
O(9A)–Pr(1)–O(1A)	118.1(1)	N(1B)–Pr(1)–O(1A)	71.1(1)
O(8B)–Pr(1)–O(1A)	74.2(1)	O(1)–Pr(1)–O(3A)	142.7(1)
O(3)–Pr(1)–O(3A)	73.2(1)	O(8A)–Pr(1)–O(3A)	69.6(1)
O(9A)–Pr(1)–O(3A)	79.5(1)	N(1B)–Pr(1)–O(3A)	143.4(1)
O(8B)–Pr(1)–O(3A)	131.8(1)	O(1A)–Pr(1)–O(3A)	74.0(1)
O(1)–Pr(1)–O(8AA)	70.0(1)	O(3)–Pr(1)–O(8AA)	69.6(1)
O(8A)–Pr(1)–O(8AA)	176.6(1)	O(9A)–Pr(1)–O(8AA)	133.1(1)
N(1B)–Pr(1)–O(8AA)	88.3(1)	O(8B)–Pr(1)–O(8AA)	110.7(1)
O(1A)–Pr(1)–O(8AA)	108.8(1)	O(3A)–Pr(1)–O(8AA)	113.4(1)
O(1)–Pr(1)–O(9AA)	118.1(1)	O(3)–Pr(1)–O(9AA)	79.5(1)
O(8A)–Pr(1)–O(9AA)	133.1(1)	O(9A)–Pr(1)–O(9AA)	144.7(2)
N(1B)–Pr(1)–O(9AA)	107.7(1)	O(8B)–Pr(1)–O(9AA)	130.2(1)
O(1A)–Pr(1)–O(9AA)	74.1(1)	O(3A)–Pr(1)–O(9AA)	72.3(1)
O(8AA)–Pr(1)–O(9AA)	48.3(1)	O(1)–Pr(1)–O(8BA)	74.2(1)
O(3)–Pr(1)–O(8BA)	131.8(1)	O(8A)–Pr(1)–O(8BA)	110.7(1)
O(9A)–Pr(1)–O(8BA)	130.2(1)	N(1B)–Pr(1)–O(8BA)	24.6(1)
O(8B)–Pr(1)–O(8BA)	49.2(2)	O(1A)–Pr(1)–O(8BA)	71.5(1)
O(3A)–Pr(1)–O(8BA)	142.6(1)	O(8AA)–Pr(1)–O(8BA)	65.9(1)
O(9AA)–Pr(1)–O(8BA)	84.6(1)	O(1)–P(1)–O(2)	115.3(1)
O(3)–P(2)–C(1)	114.2(2)	Pr(1)–O(1)–P(1)	155.2(2)
P(1)–O(2)–C(1)	121.8(2)	Pr(1)–O(3)–P(2)	153.0(2)
P(2)–C(1)–O(2)	105.0(3)	Pr(1)–O(9A)–N(1A)	99.3(3)
Pr(1)–O(8A)–N(1A)	95.3(3)	Pr(1)–N(1B)–O(10B)	180.0(1)
Pr(1)–N(1B)–O(8B)	59.1(3)	Pr(1)–N(1B)–O(8BA)	59.1(3)
Pr(1)–O(8B)–N(1B)	96.3(3)		

Table 7
Atomic coordinates for **A3** ($\times 10^4$) and equivalent isotropic displacement coefficicnts ($Å^2 \times 10^3$)

	x	y	z	U_{eq}[a]
Pr	2511(1)	2830(1)	2515(1)	35(1)
P(1)	3772(2)	3038(2)	4244(2)	37(1)
P(2)	2900(2)	4339(2)	3795(2)	47(2)
O(1)	3373(5)	2698(5)	3605(5)	45(4)
O(2)	2725(5)	3360(5)	4595(6)	59(5)
O(3)	2503(4)	3931(4)	3195(5)	43(4)
O(4)	4411(5)	3426(5)	4223(6)	60(5)
O(5)	3991(4)	2507(5)	4838(5)	54(4)
O(6)	2478(6)	4867(6)	4059(7)	92(6)
O(7)	3489(7)	4763(5)	3686(7)	81(6)
C(1)	3265(7)	3737(7)	4496(8)	46(6)
C(2)	4839(7)	3178(8)	3856(10)	61(7)
C(3)	3622(9)	1865(9)	4877(11)	73(9)
C(4)	1756(11)	4911(12)	3830(12)	106(11)
C(5)	3454(11)	5158(10)	3095(12)	101(12)
C(6)	3679(7)	4072(8)	5181(10)	45(7)
C(7)	4162(8)	4583(7)	5232(9)	58(7)
C(8)	4493(9)	4859(9)	5862(14)	91(12)
C(9)	4356(12)	4643(11)	6421(13)	94(12)
C(10)	3856(10)	4118(12)	6389(12)	86(11)
C(11)	3547(8)	3866(8)	5779(11)	52(8)
P(1A)	1257(2)	2446(2)	830(3)	55(2)
P(2A)	1481(2)	4034(2)	1097(2)	48(2)
O(1A)	1786(5)	2273(4)	1461(5)	46(4)
O(2A)	2042(5)	3272(7)	400(7)	73(5)
O(3A)	1995(5)	3828(4)	1739(5)	48(4)
O(4A)	1185(6)	1845(6)	268(6)	73(5)
O(5A)	545(5)	2545(7)	875(6)	70(5)
O(6A)	785(6)	4196(7)	1157(7)	86(6)
O(7A)	1641(7)	4706(5)	748(7)	91(6)
C(1A)	1363(7)	3309(7)	457(8)	43(6)
C(2A)	1729(10)	1433(10)	209(10)	84(10)
C(3A)	235(10)	2004(9)	1223(11)	89(10)
C(4A)	642(10)	4346(10)	1754(12)	98(12)
C(5A)	2320(10)	5022(10)	920(12)	92(11)
C(6A)	892(6)	3472(6)	−234(9)	36(6)
C(7A)	244(8)	3744(8)	−336(9)	54(8)
C(8A)	−158(9)	3869(9)	−984(11)	62(8)
C(9A)	23(9)	3718(8)	−1533(12)	60(8)
C(10A)	671(7)	3445(7)	−1442(9)	48(7)
C(11A)	1088(8)	3320(8)	−809(9)	49(8)
N(1A)	3502(6)	3419(6)	1844(10)	52(7)
O(8A)	3060(5)	2966(5)	1539(6)	50(5)
O(9A)	3521(5)	3533(6)	2457(8)	60(5)
O(10A)	3870(7)	3674(8)	1580(8)	97(7)
N(1B)	1382(7)	2869(7)	3149(12)	70(9)
O(8B)	1294(5)	2908(6)	2520(9)	65(6)
O(9B)	1954(5)	2635(6)	3493(6)	55(5)
O(10B)	973(8)	3037(9)	3405(8)	99(8)
N(1C)	2991(7)	1307(7)	2671(8)	60(6)
O(8C)	3244(5)	1772(5)	2410(6)	57(5)
O(9C)	2489(6)	1507(5)	2863(6)	56(5)
O(10C)	3224(7)	708(6)	2786(7)	96(7)

[a]Equivalent isotropic U defined as one third of the trace of the orthogonalised U_{ij} tensor.

Table 8
Atomic coordinates for **B3** ($\times 10^4$) and equivalent isotropic displacement coefficients ($Å^2 \times 10^3$)

	x	y	z	U_{eq}[a]
Pr(1)	0	−6(1)	2500	29(1)
P(1)	1508(1)	−707(1)	4683(1)	37(1)
P(2)	809(1)	2836(1)	4270(1)	40(1)
O(1)	940(1)	−863(3)	3830(2)	42(1)
O(2)	1645(1)	847(3)	5069(2)	40(1)
O(3)	463(1)	2117(3)	3431(2)	41(1)
C(1)	1213(2)	1619(4)	5180(2)	35(1)
O(4)	2097(1)	−1065(4)	4746(2)	59(1)
C(2)	2164(3)	−836(9)	4069(4)	93(4)
O(5)	1542(2)	−1663(3)	5386(2)	60(2)
C(3)	1160(3)	−2885(6)	5191(4)	78(4)
O(6)	1311(2)	3877(3)	4390(2)	70(2)
C(4)	1467(3)	4061(10)	3804(4)	109(5)
O(7)	430(2)	3738(4)	4496(2)	72(1)
C(5)	−191(2)	4196(6)	3914(3)	68(1)
C(11)	1553(2)	2365(4)	6034(2)	37(1)
C(12)	1241(2)	2665(5)	6415(2)	48(2)
C(13)	1529(2)	3452(6)	7178(3)	66(2)
C(14)	2125(3)	3868(6)	7573(3)	73(3)
C(15)	2441(2)	3549(6)	7219(3)	72(2)
C(16)	2156(2)	2795(5)	6451(3)	53(2)
N(1A)	671(2)	514(4)	1647(2)	45(2)
O(8A)	162(2)	−92(3)	1235(2)	55(2)
O(9A)	890(1)	832(4)	2421(2)	54(1)
O(10A)	945(2)	797(5)	1320(2)	73(2)
N(1B)	0	−3220(6)	2500	62(3)
O(8B)	257(2)	−2529(3)	2219(2)	57(2)
O(10B)	0	−4526(7)	2500	138(8)

[a]Equivalent isotropic U defined as one third of the trace of the orthogonalised U_{ij} tensor.

Samples of **B2** showed no decrease in weight on heating at 80 °C for 1 week whilst a crude sample of **B11** suffered a 22% weight reduction under the same conditions corresponding well with the loss of three moles of methyl nitrate. The ready loss of nitrate may explain the consistently low values obtained for nitrogen in the microanalyses (see Tables 1 and 2).

The thermal decomposition was studied by differential scanning calorimetry. Fig. 3 shows typical results for the free ligand, $La(NO_3)_3L_2$ and $La(NO_3)_3L'_2$. These results are interpreted as an endothermic event on melting for L being followed by exothermic isomerisation. For **A1** we ascribe the exothermic event to isomerisation whilst the endotherm at slightly higher temperature could correspond to simultaneous melting and loss of methyl nitrate. For the complex **B1** endothermic melting and loss of nitrate are seen.

Consistent values for the enthalpy changes for these events could not be obtained presumably due to the vigorous and irreversible nature of the decomposition and proximity of the events which all occur in a narrow temperature range.

2.4. Stability towards nitrate substitution

IR spectra of all the complexes obtained as KBr discs contained a band at 1380 cm^{-1} which corresponds

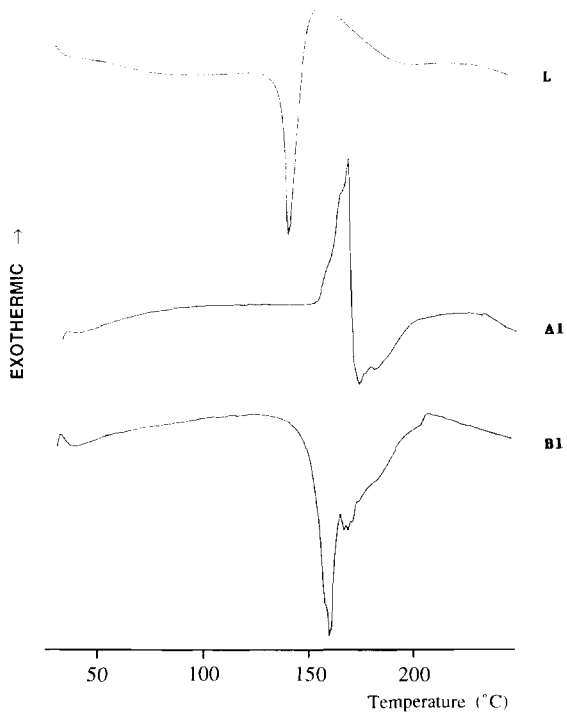

Fig. 3. Differential scanning calorimetry plots for L, **A1** and **B1**.

well with that of ionic nitrate [16]. This band tended to increase in intensity with the atomic weight of the lanthanide and for the heavier members of series **A** and **B** the bands due to coordinated nitrate were either very weak or totally absent. Spectra run as bromoform solutions show that ionic nitrate is absent thus its detection in the KBr matrix is probably due to nitrate substitution by bromide.

Interestingly, spectra run as KCl discs show that the rate of substitution is reduced. For instance the spectrum of $Er(NO_3)_3L_2$ in KCl shows bands due to bidentate nitrate whilst in KBr these peaks are reduced in intensity and the absorbance due to ionic nitrate increases. The spectrum run as a KI disc shows only ionic nitrate to be present. On heating the KCl disc to 120 °C the substitution appears to be complete. This trend in reactivities is the opposite to that which might be expected in terms of the hardness of the halide ions. Presumably the lattice energy of the potassium halide provides a kinetic barrier to the substitution reactions.

2.5. ^{31}P NMR spectra

Although NMR of paramagnetic molecules does not, in general, yield detailed structural information, analysis of the lanthanide induced shifts for a series of related complexes has been shown to give indications of changes in structure across the series of lanthanide complexes [17,18]. The lanthanide induced shifts are analysed by plotting $\delta_i/\langle S_z\rangle_i$ versus $D_i/\langle S_z\rangle_i$ and δ_i/D_i versus $\langle S_z\rangle_i/D_i$ where $\langle S_z\rangle_i$ is the spin expectation value and D_i is related to the variation in paramagnetic shift which should occur if the crystal field coefficients are independent of the lanthanide ion. $\langle S_z\rangle_i$ and D_i are characteristics of a particular lanthanide ion and their values have been calculated [19,20]. δ_i is the paramagnetic shift given by $\delta_i = \delta_{Ln} - 1/2(\delta_{La} + \delta_{Lu})$, where δ_{Ln} is the observed shift for a given lanthanide and δ_{La} and δ_{Lu} are the shifts of the diamagnetic lanthanum and lutetium complexes. If the complexes are essentially isostructural across the series, then both plots are expected to be linear, whilst if a major structural change occurs, for example a change of coordination number or a change from monodentate to bidentate coordination of a ligand, then both plots are expected to show a break. Minor changes in structure are implied if the plot of $\delta_i/\langle S_z\rangle_i$ versus $D_i/\langle S_z\rangle_i$ shows a break whilst δ_i/D_i versus $\langle S_z\rangle_i/D_i$ remains linear. The results for series **A** are shown in Fig. 4 whilst the results for both phosphorus nuclei in series **B** are shown in Fig. 5. The plots generally

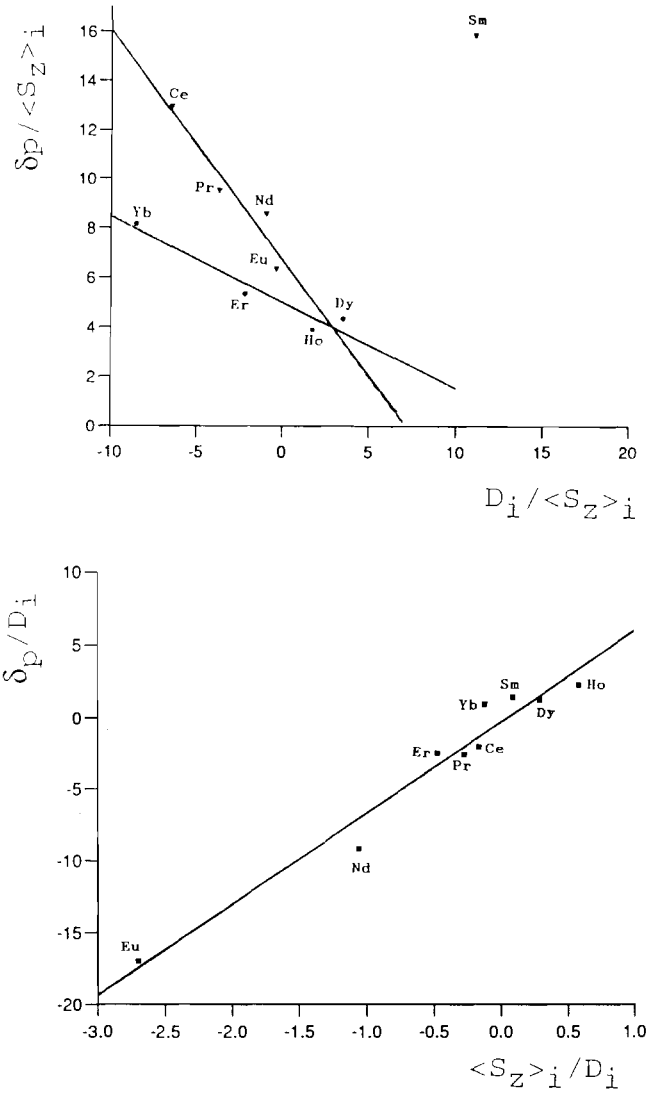

Fig. 4. Lanthanide induced shift plots for series **A**.

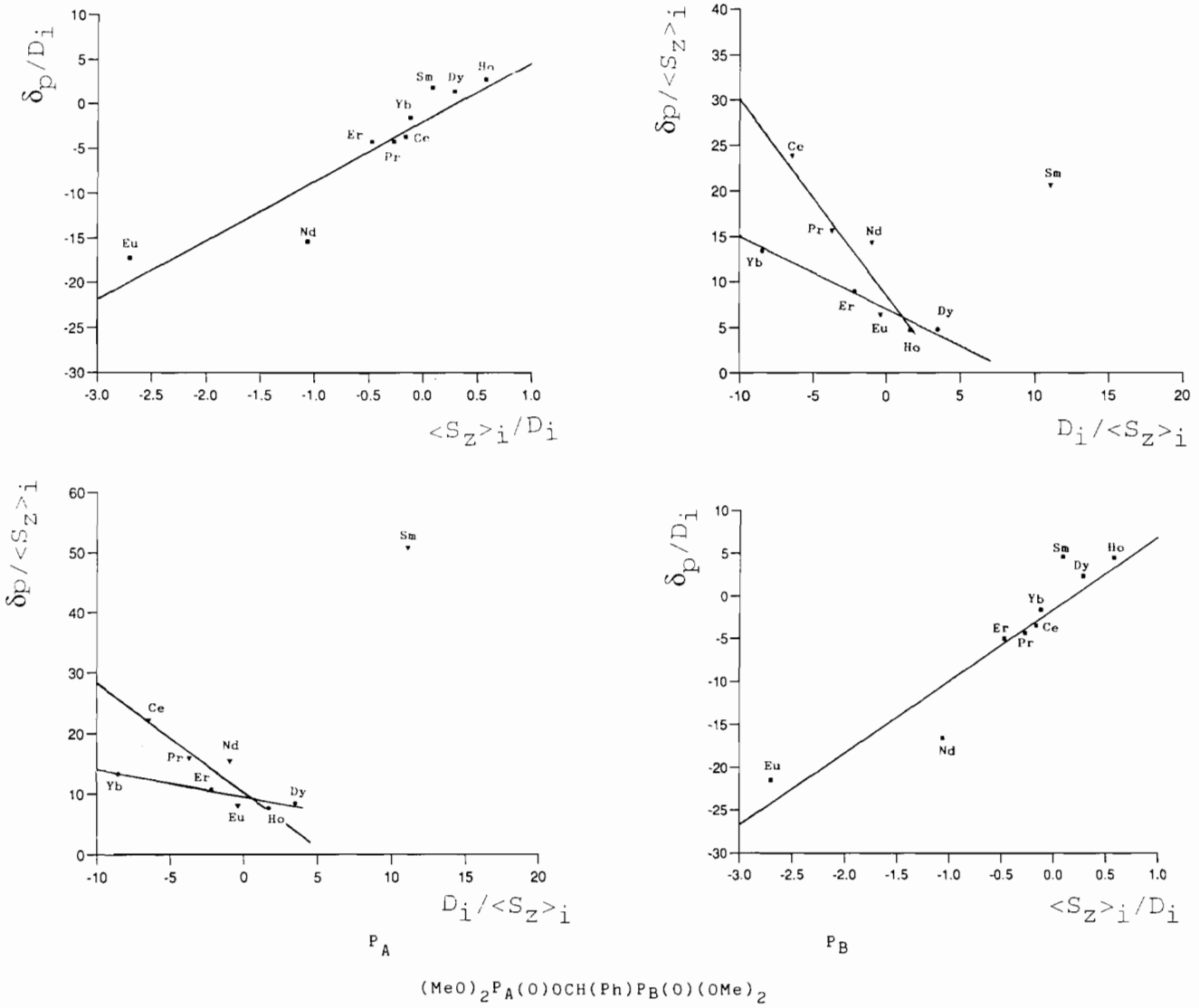

Fig. 5. Lanthanide induced shift plots for series **B**.

show good linearity, particularly if the value for samarium is disregarded. The unreliability of the values for samarium could be due to the fact that the shifts tend to be similar in magnitude to those of the lanthanum and lutetium complexes thus δ_i is often in the region of zero and small errors in any of the measured shifts could lead to a large relative error in the subsequently calculated values. This coupled with the small values of D_i and, in particular $\langle S_z \rangle_i$ for samarium would tend to magnify these errors. Similar effects have been noted previously [17,18].

For both series **A** and **B** the results of the analysis of the lanthanide induced shifts are the same. The plot of δ_i/D_i versus $\langle S_z \rangle/D_i$ is linear whilst the plots of $\delta_i/\langle S_z \rangle$ versus $D_i/\langle S_z \rangle$ show two distinct lines with a break between the lighter and heavier lanthanides. It seems that the complexes **A** and **B** for lanthanum to europium are isostructural whilst those of dysprosium to lutetium form a separate isostructural series. The differences between the complexes of heavier and lighter lanthanides appear, however, to be minor. Although it is not possible to be correlate solution data with solid state information with certainty, the break in solution structure does coincide with a minor change in the IR spectra in the nitrate N–O stretch region for the **B** complexes where the doublet in the 1300 cm^{-1} region observed for the La to Gd complexes becomes a singlet for the subsequent complexes.

3. Experimental

The ligand L was prepared by the published procedure [9]. δ ^{31}P ($CDCl_3$) 17.9 (lit. 18.0 [9]). L′ was prepared by treating a methanol solution of L with a trace of triethylamine [8]. Evaporation of the solvent gave a

colourless oil which was used without further purification. δ ^{31}P ($CDCl_3$) 18.7, 1.0 ^3J(PP) 33 Hz (lit. δ ^{31}P 21.9 ^3J(PP) 29) [8].

The general methods for preparation of the complexes were described in Section 2 and so detail is given below for only some representative syntheses for complexes of each series. All complexes had the characteristic colour of the lanthanide ion.

3.1. Series A

A3; *$Pr(NO_3)_3L_2$*. $Pr(NO_3)_3 \cdot 5H_2O$ (0.33 g, 0.79 mmol) in acetonitrile (5 ml) was added to a slurry of the ligand (0.52 g, 1.57 mmol) in 5 ml acetonitrile at 0 °C. The ligand dissolved on mixing to give a clear solution from which the product precipitated spontaneously as green crystals (0.58 g, 75%).

A8; *$Dy(NO_3)_3L_2$*. $Dy(NO_3)_3 \cdot 6H_2O$ (0.34 g, 0.74 mmol) in acetonitrile (5 ml) was added to a slurry of the ligand (0.50 g, 1.54 mmol) at 0 °C. The resulting clear solution was evaporated under reduced pressure and the resulting crude product recrystallised from dichloromethane/diethyl ether to give the product as a white solid (0.48 g, 65%).

*Attempted preparation of **A10***; *$Er(NO_3)_3L_2$*. $Er(NO_3)_3 \cdot 5H_2O$ (0.34 g, 0.77 mmol) in acetonitrile (5 ml) was added to a suspension of the ligand at 0 °C. The resulting clear pink solution was evaporated under reduced pressure without external warming. Following trituration with diethyl ether the resulting pale pink powder did not give satisfactory elemental analysis. The crude material was dissolved in chloroform and diethyl ether carefully added to form two layers which were allowed to slowly diffuse over two weeks. The resulting pink crystals gave the following analysis. *Anal.* Found: C, 21.88; H, 3.47; N, 4.33. Calc. for $Er_2O(NO_3)_4L_2$: C, 21.19; H, 2.91; N, 4.49%.

*Attempted preparation of **A9***; *$Ho(NO_3)_3L_2$*. When holmium nitrate was treated as described above pale orange crystals were obtained which gave the following composition. *Anal.* Found: C, 21.93; H, 3.31; N, 4.60. Calc. for $Ho_2O(NO_3)_4L_2$: C, 21.27; H, 2.92; N, 4.51%.

3.2. Series B

B1; *$La(NO_3)_3L'_2$*. $La(NO_3)_3 \cdot 6H_2O$ (1.0 g, 2.41 mmol) in 20 ml acetonitrile was treated with the ligand (1.61 g, 4.97 mmol). The solvent was evaporated to 5 ml under reduced pressure and the product was precipitated as a white solid by addition of diethyl ether (2.07 g, 88%).

B6; *$Eu(NO_3)_3L'_2$*. $Eu(NO_3)_3 \cdot 5H_2O$ (0.18 g, 0.42 mmol) was dissolved in acetonitrile (5 ml) and L′ (0.30 g, 0.93 mmol) was added. The solution was evaporated under reduced pressure and the resulting solid recrystallised from chloroform/diethyl ether to give the product as colourless crystals (0.23 g, 55%).

*Attempted preparation of **B10***; *$Er(NO_3)_3L'_2$*. $Er(NO_3)_3 \cdot 5H_2O$ (0.34 g, 0.77 mmol) was stirred in acetonitrile and the mixture evaporated under reduced pressure to give a pink oil. Recrystallisation from chloroform/diethyl ether gave a pale pink powder. *Anal.* Found: C, 20.38; H, 3.40; N, 4.30. Calc. for $Er_2(OH)_2(NO_3)_4L'_2$: C, 20.89; H, 3.03; N, 4.43%.

*Attempted preparation of **B11***; *$Yb(NO_3)_3L'_2$*. The same procedure using ytterbium nitrate gave a white solid with the following composition. Anal. Found: C, 20.28; H, 3.30; N, 4.27. Calc. for $Yb_2(OH)_2(NO_3)_4L'_2$: C, 20.70; H, 3.00; N, 4.39%.

The ^{31}P NMR spectra were recorded at 36.23 MHz on a JEOL FX90Q spectrometer. IR spectra were recorded on a Perkin-Elmer 457. Differential scanning calorimetry was performed an a Mettler DSC 25.

3.2. Crystallography

Crystals of **A3** suitable for single crystal work formed spontaneously on mixing the reagents. Crystal data: **A3**, $C_{22}H_{34}N_3O_{23}P_4Pr$, $M_r = 973.3$, monoclinic space group $C2/c$, $a = 21.011(8)$, $b = 18.708(8)$, $c = 20.721(5)$ Å, $\beta = 107.91(1)°$, $U = 7750(6)$ Å^3, $Z = 8$, $D_c = 1.668$ Mg/m^3, $\mu = 1.509$ mm^{-1}, $F(000) = 3920$. The crystal dimensions were $0.49 \times 0.28 \times 0.18$ mm. The intensities of 5326 unique reflections with $2\theta < 54°$ were measured with a Siemens P4 diffractometer with graphite monochromated Mo Kα radiation ($\lambda = 0.71073$ Å) using an ω-scan technique. The data were corrected for Lorentz and polarisation effects to yield 3453 unique reflections with $F > 4.0\sigma(F)$.

The structure was solved by Patterson methods, and refined using SHELXTL PC [21]. The hydrogen atoms of the hydroxyl groups were not located. All other hydrogen atoms were included in calculated positions with a single fixed thermal parameter. The non-hydrogen atoms were refined with anisotropic thermal parameters.

Final cycles of refinement employed a weighting parameter $g = 0.0123$ in $w = 1/(\sigma^2(F) + gF^2)$ and gave residual indices $R = \Sigma(|F_o| - |F_c|)/\Sigma|F_o| = 0.069$ and $R' = [\Sigma w(|F_o| - |F_c|)^2/\Sigma w|F_o|^2]^{1/2} = 0.085$. The final difference Fourier map had a +1.9 e Å^{-3} peak at <1 Å from phosphorus and a 1.6 e Å^{-3} peak 0.75 Å from praseodymium. An analysis of the weighting scheme over $|F_o|$ and sin θ/λ showed that the weighting of high angle reflections was too great, and the most significant deviations were reflections having high h, k and l values with $|F_o| > |F_c|$.

Suitable crystals of **B3** were grown by slow evaporation of a toluene/dichloromethane solution. Crystal data: **B3**, $C_{22}H_{34}N_3O_{23}P_4Pr$, $M = 973.3$, monoclinic space group $C2/c$, $a = 26.493(3)$, $b = 9.3020(10)$, $c = 18.884(2)$ Å, $\beta = 124.560°$, $U = 3832.5(7)$ Å^3, $Z = 4$, $D_c = 1.690$ Mg/

m^3, $\mu = 1.526$ mm^{-1}, $F(000) = 1968$. The crystal dimensions were $0.44 \times 0.41 \times 0.36$ mm. The intensities of 6537 unique reflections with $2\theta < 59.8°$ were measured with a Siemens P4 diffractometer with graphite monochromated Mo Kα radiation ($\lambda = 0.71073$ Å) using an ω-scan technique. The data were corrected for Lorentz and polarisation effects to yield 5530 reflections with $F > 4.0\sigma(F)$.

The structure was solved by Patterson methods, and refined using SHELXTL PC [21]. All hydrogen atoms were included in calculated positions with a single fixed thermal parameter. The non-hydrogen atoms were refined with anisotropic thermal parameters.

Final cycles of refinement employed a weighting parameter $g = 0.0007$ in $w = 1/(\sigma^2(F) + gF^2)$ and gave residual indices $R = \Sigma(|F_o| - |F_c|)/\Sigma|F_o| = 0.0393$ and $R' = [\Sigma w(|F_o| - |F_c|)^2/\Sigma w|F_o|^2]^{1/2} = 0.0572$. The largest difference peaks are $+1.7$ e Å^{-3}, 0.7 Å from O7 perpendicular to the P2–O7–C5 plane.

4. Supplementary material

Additional material available from the Cambridge Crystallographic Data Centre comprises H atom coordinates, thermal parameters and the remaining bond lengths and angles.

Acknowledgements

We thank the SERC for the use of the CSSR Data base at the Daresbury laboratory. We also thank ICI Organics (Blackley) for some financial assistance.

References

[1] R.D. Gillard, G. Wilkinson and J. McCleverty (eds.), *Comprehensive Coordination Chemistry,* Vol. 3, Pergamon, London, 1987.
[2] M. Chmutova, N.E. Kochetkova and B.F. Myasoedov, *J. Inorg. Nucl. Chem., 42* (1980) 892.
[3] A.M. Rozen, Z.I. Nikolotova, N.A. Kartasheva and K.S. Yudina, *Dokl. Akad. Nauk. SSSR, 222* (1975) 604.
[4] G.V. Tsintsadze, V.V. Skopenko, T.M. Kublashvili and L.B. Kereselidze, *Ukr. Khim. Zh., 46* (1980) 363.
[5] G.V. Tsintsadze, T.I. Tsivisivadze, F.V. Orbelatsze, A.A. Dvorkin and T.M. Kublashvili, *Nauch. Tr. GR. Pol. Inst. Lenina,* (1985) 60.
[6] T.H. Siddall, *J. Inorg. Nucl. Chem., 25* (1963) 883.
[7] A.W.G. Platt, *Polyhedron, 12* (1993) 467.
[8] A. Tromelin, D. El Manouni and R. Burgada, *Phosphorus Sulfur, 27* (1986) 301.
[9] D.A. Nicholson and H. Vaughn, *J. Org. Chem.,* (1971) 36.
[10] L. Yong-Hua, H. Ning-Hai, Z. Qing-Lian, L. Shu-Zhen, W. Shi-Xue, S. En-Dong and W. Ming-Yi, *Acta Chem. Sinica, 42* (1984) 372.
[11] T.J.R. Weakley, *Acta Crystallogr., Sect. C, 45* (1989) 525.
[12] L. Fupei and J. Zhong, *J. Chin. Rare Earth Soc., 7* (1989) 1.
[13] Y. Leroux, D. El Manouni, A. Safsaf, A. Neuman, H. Gillier and R. Burgada, *Phosphorus, Sulfur Silicon, 56* (1991) 95.
[14] J. Laane and J.R. Ohlsen, *Prog. Inorg. Chem., 27* (1980) 465.
[15] J.C.D. Brand and T.M. Cawthon, *J. Am. Chem. Soc., 77* (1955) 319; B.M. Gatehouse, S.E. Livingstone and R.S. Nyholm, *J. Chem. Soc.,* (1957) 4222.
[16] K. Nakamoto, *Infrared and Raman Spectra of Inorganic and Coordination Compounds,* Wiley, New York, 1986.
[17] J.A. Peters, *J. Magn. Reson., 68* (1986) 240.
[18] P. Rubini, C. ben Nasr, L. Rodehuser and J-J. Delpuech, *Magn. Reson. Chem., 25* (1987) 609.
[19] R.M. Golding and M.B. Hatton, *Aust. J. Chem., 25* (1972) 2577.
[20] R.M. Golding and P. Pyykko, *Mol. Phys., 26* (1972) 1389.
[21] G.M. Sheldrick, *SHELXTL,* PC Version 4.2, Siemens Analytical X-Ray Instruments, Madison, WI, 1991.